Sl. No.	IIT Ropar List of Recent Publications with Abstract Coverage: February, 2026
A	**Book Chapter(s)**
1.	Biotechnological advances in therapeutics: Therapeutic proteins, antibodies, vaccines, and regulatory standards **M Kumar, P Shukla, M Bhatt, B Das** - Industrial Microbiology and Biotechnology: Trends in Microbial Biotechnology: Book Chapter, 2026 **Abstract:** Therapeutic proteins are engineered proteins used to treat or prevent diseases such as cancer, diabetes, and cardiovascular disorders by replacing missing proteins, enhancing existing pathways, or novel functions. Therapeutic proteins include haemostasis factors, thrombolytic agents, hormones, and recombinant vaccines. The development of chimeric and humanised antibodies, along with antibody fragments, has a crucial role in modern therapeutics by enhancing precision treatment and minimising immune rejection. It also emphasises microbial transformation processes and cell surface display technologies that enhance drug development and delivery mechanisms. Vaccine development includes DNA-based approaches, along with efficient ways to produce antibodies and enzymes on a large scale. Hence, DNA-based vaccines have become a valuable technique for protecting against infectious diseases. Current Good Manufacturing Practice (cGMP) and Good Laboratory Practice (GLP) guidelines ensure that research and production are done safely, correctly, and meet quality standards. This chapter highlights the in-depth knowledge about therapeutic proteins and their classes, biotechnology, microbiology, chimeric and humanised antibodies, and their therapeutic applications.
2.	Enhancing security in smart environments using deep learning: A comprehensive approach SI Yaqoob, P Kamal, **S Aggarwal,** A Kanade, S Kanade - Deep Learning for Intrusion Detection: Techniques and Applications: Book Chapter, 2026 **Abstract:** Smart environments are networks of systems and devices that offer ease on a previously unseen level but, of course, also threaten new openings in security lapses. This chapter discusses the exploitation of deep learning techniques in strengthening security protocols in smart environments. The chapter begins with a brief overview of smart environments and the issues of security they bring into the picture and then deep-dives into how well deep learning can solve those issues. This chapter lays down and describes several deep learning models—such as GANs, RNNs, and CNNs among others—and how they could be used for enhancing security protocols. It uses case studies and real data to illustrate the strength of deep learning algorithms for prediction of threats, detection of anomalies, and intrusion detection. This chapter reviews possible usage of deep learning alongside edge computing and blockchain to form robust security frameworks. It further analyses its function in the framework for proactive defense against novel threats. The chapter goes a step further and explains challenges with considerations for deploying deep learning for security in smart environments with interpretability, scalability, and data privacy issues. It gives ways of dealing with the said challenges and identifies the multidisciplinary involvement of practitioners in machine learning and security experts. It ends with this chapter as it reminds everyone that deep learning revolutionizes the reinforcement of security protocols in intelligent environments by using advanced algorithms and innovative methods to allow stakeholders better proactive protection for vital infrastructures and thus ensure resilience and integrity of intelligent ecosystems.
3.	Life cycle assessment of biomass waste management processes V Pandey, S Gupta, M Kumar, **J Singh,** D Joshi - Sustainable Technologies for Value Addition to Biomass Waste: Book Chapter, 2026

	Abstract: As the global demand for sustainable waste management and renewable energy intensifies, life cycle assessment (LCA) emerges as a critical tool for evaluating the environmental footprint of biomass waste management systems. This chapter provides a comprehensive analysis of various waste-to-energy technologies, including anaerobic digestion, incineration, gasification, composting, and pyrolysis assessing their greenhouse gas emissions, energy efficiency, and resource recovery potential. The research underscores the environmental trade-offs inherent in these technologies and explores their integration into circular economy frameworks to maximize sustainability. Additionally, the chapter examines emerging innovations such as integrated biorefineries and biochar production, highlighting their transformative role in mitigating climate change and enhancing resource efficiency. By leveraging LCA methodologies, this chapter offers invaluable insights for policymakers, industries, and researchers in shaping data-driven, eco-efficient waste management strategies. Ultimately, it advocates for a paradigm shift toward holistic, science-based decision-making to drive the transition to a low-carbon, sustainable future.
4.	The role of micronutrients in managing breast cancer: Implications of supplementation therapies on molecular and cellular signaling pathways MS Sibian… **V Aggarwal** - Functional Biochemistry of Micronutrients: Book Chapter, 2026 **Abstract:** Breast cancer has emerged as a significant global health concern in recent years, making the prevention of this disease dependent on various chemotherapeutic and alternative therapy options. Micronutrients, including vitamins and minerals and plant-derived bioactive components, play a crucial role in the body through gene expression, cellular growth, and immunomodulation. It is well known that certain micronutrients, such as vitamins A, B, C, D, and E, coenzyme Q10, omega-3 fatty acids, and minerals like Se, Zn, Fe, Mg, and Cu, serve multifunctional roles in cancer development or suppression, depending on their systemic concentration and bioavailability. Some micronutrients may act as inhibitors, while others could function as potential tumor promoters due to their roles in gene regulation and cellular signaling transduction. Micronutrients can regulate key cancer signaling pathways, including the PI3K-AKT, MAPK, and JAK-STAT pathways, thereby controlling cell proliferation, apoptosis, and immune function. Hence, interventions with micronutrients are potential therapeutic options for the management of breast cancer. The significance of micronutrient therapy in breast cancer prevention also arises from their epigenetic control of gene expression. This chapter provides a comprehensive understanding of the efficacy of micronutrient-based interventions for preventing breast cancer.
B	**Conference Proceeding(s)**
5.	A fast and reliable hall sensor fault detection technique for BLDC motor drives **V Kumar, AVR Teja** - 2025 IEEE 4th Industrial Electronics Society Annual On-Line Conference (ONCON), 2026 **Abstract:** This paper presents a novel method for fault detection of any one of the hall sensors of the BLDC motor with the sum of the product of current and the hall sensor output. This method is not only simple to implement but also detects the fault almost instantaneously in both starting and running conditions of the bldc motor drive. Further, the proposed method also provides the information about which hall sensor has failed along with the detection of fault. The proposed method is tested in simulation using MATLAB/Simulink software in a variety of hall sensor fault test cases and the results are presented. It is found that the fault detection is successful in all possible test cases of hall sensor fault and the detection is done within 0.2 s.
6.	A novel islanding detection framework using synchrophasor data sharing K Chauhan, R Prakash, VK Gaur, **Y Bansal, R Sodhi** - IEEE 5th International Conference on Sustainable Energy and Future Electric Transportation, 2026

	Abstract: This paper proposes a novel distributed islanding detection framework that enhances situational awareness in active distribution networks through synchrophasor-based data sharing among micro-phasor measurement units (μPMU). A strategically deployed μPMU network is considered, where each unit exchanges real-time frequency measurements with its two nearest neighbors through a ring-topology communication structure. A novel islanding detection index (termed as pidx) is computed at each μPMU node using the p−value, a probabilistic measure derived from the analysis of variance (ANOVA) of shared frequency data. ANOVA operates under the null hypothesis that the means of all frequency vectors are equal. A pidx value below 0.05 indicates a statistically significant deviation, leading to the rejection of the null hypothesis and confirming an islanding event. The proposed framework is validated on the IEEE 33-bus distribution system with four distributed generation (DG) units under diverse islanding and non-islanding scenarios in PSCAD/EMTDC. The results demonstrate the effectiveness, scalability, and robustness of the method in accurately distinguishing islanding events, making it well-suited for modern power systems with high DG penetration.
7.	A novel SHE-PWM switching angle correction technique in five level CHB inverters with varying DC sources **MK Meena, AVR Teja** - 2025 IEEE 4th Industrial Electronics Society Annual On-Line Conference (ONCON), 2026 **Abstract:** In this paper, a novel approach to restore fundamental output voltage along with harmonic elimination in SHE PWM-based five-level cascaded h-bridge inverters having two switching angles and two varying DC sources is presented. By modifying both the SHE switching angles obtained with fixed DC voltages, the proposed technique eliminates chosen harmonic from the output and restores the fundamental output even in the presence of DC variations. The proposed method requires less memory and computation to implement. This approach is evaluated in simulation for different possible cases of DC voltage variation in five level inverters using MATLAB/Simulink. The results demonstrate that, even in the presence of practical DC sources till 20% variation, the proposed approach reliably restores the intended output voltage and effectively eliminates selected harmonic.
8.	Anomaly detection and mitigation in multi-agent AGC and HVDC integrated power system using machine-learning technique **S Beura, A Kumar, BP Padhy** - 2025 IEEE 5th International Conference on Sustainable Energy and Future Transportation, 2025 **Abstract:** Cyber-physical systems (CPSs) are opening new avenues for increased reliability, efficient control, and greater connectivity amongst power system elements in the twenty-first century. Therefore, the greatest attention must be given to preventing the manipulation of this system through foreign interventions such as fake data insertion (FDI). Phasor measuring units (PMUs) are used in power system monitoring to provide additional information about the system's transient performance. PMU measures, such as frequency and tie-line power variations, aid in determining the necessary generation adjustments. PMU measurements synthesize the control signals for high-voltage DC lines' power modulation controllers (PMC) and automated generation control (AGC) units. Any FDI-style attack on these devices, however, has the potential to weaken line overload and generator limitations, jeopardizing the overall stability of the power system. In this paper, we work on the IEEE 39 bus system for attack detection using transformer neural networks (TNNs) and Extreme Gradient Boosting (XGBOOST) detectors in the presence of an attack. The proposed work considers three inter-area power controller (IPC) units that control the respective area's generations and a PMC controller HVDC line.
9.	Intuitionistic fuzzy graph embedded random vector functional link with multiview learning

	V Ahire, Y Kumar, MA Ganaie - International Joint Conference on Neural Networks (IJCNN), 2025 **Abstract:** Random Vector Functional Link (RVFL) networks are popular due to their fast training and universal approximation capabilities. However, RVFL models face challenges in preserving geometric relationships and utilizing multiple feature views effectively. To address these limitations we propose the Intuitionistic Fuzzy Graph Embedded Random Vector Functional Link with Multiview Learning (IFGRVFL-MV) model. The proposed approach comprises three key components: intuitionistic fuzzy sets for uncertainty handling, graph embedding to capture intrinsic geometric structures, and multiview learning to use complementary information from multiple feature spaces. The model assigns intuitionistic fuzzy membership and non-membership values to data points making it robust to outliers. Also, the graph embedding framework preserves topological structures, increasing the generalization performance. We performed experiments on benchmark datasets from UCI and KEEL repositories which concludes that IFGRVFL-MV outperforms existing models in classification accuracy. Our results establish that IFGRVFL-MV is a promising advancement in the domain of uncertainty and multiview environments.
10.	Modified SHE for binary and trinary asymmetric CHB inverters with varying DC sources **MK Meena, AVR Teja** - 2025 IEEE 4th Industrial Electronics Society Annual On-Line Conference (ONCON), 2026 **Abstract:** This paper presents a novel approach to restore fundamental output voltage in SHE PWM-based binary and trinary asymmetric cascaded h-bridge inverters having varying DC sources. By modifying any one available SHE switching angle obtained with fixed DC voltages, the proposed technique restores the fundamental output even in the presence of DC variations. This method is tested in simulation for several possible scenarios of DC voltage variation in asymmetric CHB inverters using MATLAB/Simulink. The results show that the proposed method consistently restores the desired output fundamental voltage even in the presence of practical DC sources.
11.	ReLEaRN: Reinforcement learning enhanced profitable rebalancing in payment channel networks **S Mishra, M Bhuria, H Singla, S Pal**, I Woungang - 2025 21th International Conference on Wireless and Mobile Computing, Networking and Communication, 2025 **Abstract:** Payment Channel Networks (PCNs) act as a foundational layer in blockchain and deal with the scalability issues. However, a major challenge that continues to hinder the world-wide acceptance of PCNs is the transaction failure rate caused by channel dependency. This depletion occurs due to the dependency of PCNs on network topology. Due to this, effective node placement is crucial for establishing economical channels and strengthening network robustness. On one hand, node attachment is necessary to bring back the PCNs to a balanced state, while on the other hand, the network is prone to getting trapped in a local optimum. To address these challenges, ReLEaRN is proposed as a node placement strategy that deals with the rebalancing problem of PCNs and the local optimum problem using the Soft-Actor critic (SAC) algorithm. We simulated our proposed algorithm on topologies of the Lightning Network and achieved 90 % improvement in execution time when compared with ProfitPilot. The execution time is similar to basic heuristic topologies present in the Lightning Network, but the probability of fees collection is improved to 40 % compared to these topologies.
12.	Shapedistill: Shape-constrained knowledge distillation for medical segmentation **U Niyaz, DR Bathula** - Eighteenth International Conference on Machine Vision (ICMV 2025), 2026

	Abstract: Deploying high-quality deep learning models for medical image segmentation in remote or resource-constrained environments remains a significant challenge due to limited computational resources and infrastructure. In this work, we introduce a shape-aware model compression framework that enhances segmentation performance while ensuring model efficiency. Central to our approach is a novel FiLM-attention-based Variational Autoencoder (VAE), trained directly on ground truth masks to learn compact and expressive latent representations of anatomical structures. The decoder incorporates both Feature-wise Linear Modulation (FiLM) and spatial attention mechanisms to enable robust reconstruction and preserve global shape information. We then apply a two-stage knowledge distillation process: first, we transfer structural knowledge from the shape-aware VAE to a U-Net segmentation model (teacher); second, we distill this shape-constrained teacher into lightweight student networks. These student models inherit both semantic precision and anatomical coherence, maintaining high segmentation accuracy and shape consistency. Across four benchmark datasets, our Shape-Constrained (SC) models demonstrated consistent improvements over baseline U-Net architectures. Specifically, they achieved average IoU gains of +4.5%, +4.4%, and +4.0%, and DSC gains of +1.3%, +1.2%, and +1.7% with ResNet34, ResNet18, and MobileNet backbones, respectively.
13.	Understanding operating conditions of battery electric buses in urban public transport system of Chandigarh, India, using real-world data **J Singh,** N Gautam - IEEE 5th International Conference on Sustainable Energy and Future Electric Transport system, 2026 **Abstract:** This study aims to understand the battery electric bus operating conditions of the urban public transport system in Chandigarh, India. This study uses a real-world dataset of 78 electric buses on 36 routes. Route characteristics, including average trip speed, average passenger count, trip duration, trip length, and number of bus stops, are characterized and visualized to gain insights into their variation. The insights gained from this analysis will be instrumental for planning charging infrastructure, estimating trip energy demand, and meeting the operational requirements necessary for the electrification of urban public transport systems.
14.	When agents are powerful: Black hole search in time-varying graphs **T Kaur, A Saxena** - International Conference on Distributed Computing and Intelligent Technology, 2026 **Abstract:** A black hole is a harmful node in a graph that destroys any resource entering it, making its identification a critical task. In the *Black Hole Search (BHS)* problem, a team of agents operates on a graph G with the objective that at least one agent must survive and correctly identify an edge incident to the black hole. Prior work has addressed BHS in arbitrary dynamic graphs under the restrictive *face-to-face* communication, where agents can exchange information only when co-located. In this work, we strengthen the capabilities of agents in two ways: (i) *global communication*, and (ii) *1-hop visibility*. These enhancements lead to more efficient solutions for the BHS problem in dynamic graphs.
15.	When explainability meets vision AI: Analyzing CNNs, transformers, and state-space models in healthcare U Varman… **A Kumar,** SK Singh - 2025 International Joint Conference on Neural Networks (IJCNN), 2025 **Abstract:** Ensuring reliability and interpretability in AI-driven medical imaging is vital for fostering trust in healthcare applications. Deep learning models, including Convolutional Neural Networks (CNNs), attention-based Transformers, and Mamba-based state-space models, have demonstrated significant advancements in classification performance. However, their black-box nature necessitates rigorous explainability analysis to ensure transparency and reliability. In this

	study, we systematically evaluate the classification performance of these architectures across three medical imaging datasets: BreakHis for histopathology (at multiple magnifications), Chest X-ray for pulmonary disease classification, and Retinal images for ocular disease diagnosis. We employ gradient-based and attention-based post-hoc explainability techniques, including Grad-CAM, Grad-CAM++, and attention rollout mechanisms, to interpret model decisions and visualize feature attributions. The results reveal that CNNs, particularly MobileNetv2 and ResNet50, excel in datasets requiring fine-grained feature extraction, whereas Transformers demonstrate superior performance in tasks emphasizing global dependencies, such as Chest X-ray analysis. Mamba-based models, such as EfficientViM, provide a balance between computational efficiency and interpretability, effectively capturing long-range dependencies in complex datasets like Retinal images. By analyzing decision-making patterns and feature attribution maps, we highlight the trade-offs between classification accuracy, computational efficiency, and model interpretability. Our findings offer actionable insights for selecting task-specific AI architectures, ensuring a balance between performance and transparency, and paving the way for the deployment of trustworthy AI in medical diagnostics.
C	**Article(s)**
16.	A comprehensive activation analysis of fusion-fission cross-sections for 14N+ 175Lu system SK Gautam…**PP Singh**… R Prasad - Nuclear Physics A, 2026 Abstract: The experiments for measuring the cross sections of 35 fission-like residues (with mass numbers $74 \leq A \leq 111$) and 10 fusion-like residues have been carried out at energies ≈ 72.7 MeV, 80.3 MeV and 88.0 MeV. In this measurement, the recoil catcher technique followed by an off-beam activation γ-ray spectroscopy is used. The analysis of fusion cross-section data with code PACE4 reveals the contribution of complete and incomplete fusion processes in $^{14}N + ^{175}Lu$ reactions. Fission fragments produced as a result of fusion of ^{14}N projectile with ^{175}Lu target have also been confirmed by comparing the values of post-fission observables viz., mass (σ_A) and charge (σ_Z) dispersions (deduced from the isotopic mass and isobaric yield distributions) with literature data. In addition to this, the statistical scission-point model based theoretical calculations performed (as per the prescription of Gubbi et. al., [31]) for determining the charge dispersion (σ_Z) of Br and Kr isotopes validate the experimental values of σ_Z obtained from the isobaric yield distribution. Thus, the consistency between theoretical and experimental values of charge dispersion (σ_Z) indicates the production of fission fragments from a equilibrated compound nucleus $^{189}Pt^*$ in $^{14}N + ^{175}Lu$ reactions. In the present work, an alternative method is used for converting isotopic mass distribution into isobaric yield distribution. Furthermore, the experimental finding of mass variance (σ_M^2) of fission fragments also complements the investigations of mass (σ_A) and charge (σ_Z) dispersions, as width of mass distribution (i.e., mass variance, σ_M^2) of fission fragments is found to be exponentially function of excitation energy, hence, temperature of equilibrated compound nucleus.
17.	A loss-aware element selection framework for unit-cell splitting in energy harvesting reconfigurable intelligent surfaces **P Rattanpal, A Sharma** - IEEE Transactions on Green Communications and Networking, 2026 **Abstract:** Reconfigurable Intelligent Surfaces (RISs) offer a low-cost, energy-efficient alternative to conventional repeaters and relays, enhancing wireless coverage and spectral efficiency through dynamic electromagnetic wave manipulation. The potential of a self-powered RIS is explored in the literature by employing element splitting (ES) on the RIS surface. This approach allocates some elements for beam steering, while the remaining elements are used for RF energy harvesting (EH) to meet RIS energy needs, aiming to create self-sustainable communication systems. The heuristic algorithms existing in the literature for such element allocation are valid only for ideal

	EH circuits, therefore, the proposed work incorporates combiner losses into the analysis to identify the most effective algorithm for maintaining system performance in terms of maximizing signal-to-noise ratio (SNR) and meeting the energy requirements of the RIS. Subsequently, the analysis reveals the necessity for a new loss-aware element selection algorithm (LA-ESA), which is proposed in this work. The results finally underscore the need for an innovative architectural paradigm shift in developing self-powered RIS, particularly in light of combiner losses. This shift is anticipated to enable a more robust software solution for self-powered RIS that meets hardware needs, thereby advancing the concept of self-sustainability and supporting environmentally friendly innovations in wireless communication.
18.	A quercetin nanocarrier-loaded dual network injectable hydrogel for mesenchymal stem cells (MSCS) delivery targeting osteoarthritis **A Mukherjee, S Mitra,** N Chaudhuri, RK Sodhi, K Mukherjee, **B Das** - Small, 2026 **Abstract:** Osteoarthritis (OA) is a progressive, chronic disorder of the musculoskeletal system affecting more than 500 million individuals globally. Current treatment strategies primarily provide palliative care, with limited potential to alter disease progression or reverse tissue deterioration. Stem cell transplantation holds promising results. But poor cell retention and survival due to ROS and inflammation in OA lead to subpar therapeutic outcomes. In this study, we developed a dual-network gelatin methacrylate (GelMA) and κ-carrageenan-based injectable hydrogel loaded with antioxidant quercetin-PLGA nanoparticles for stem cell delivery to treat OA. Physicochemical studies demonstrated stable gelation, controlled degradation, and self-healing properties. In vitro studies revealed that the sustained release of quercetin effectively scavenged intracellular ROS, reduced the expression of pro-inflammatory factors such as IL6, COX2, NFκβ, and TNFα, and increased the expression of TGFβ, IL4, SOX9, COL2, and ACAN, which are responsible for inflammation control and cartilage tissue regeneration. The sustained release of nanoparticles also enhanced the M1-to-M2 macrophage transition and collagen II deposition. In vivo studies demonstrated that the nanoparticle-loaded stem cell-encapsulated hydrogel increased glycosaminoglycan deposition, reduced inflammation, and improved joint mobility and cartilage repair. Thus, this antioxidant hydrogel-based cell delivery system demonstrated suitability for OA therapy.
19.	A step closer towards the digital twin of the plant **K Singh,** AE Saddik, M Saini - ACM Transactions on Multimedia Computing, Communications and Applications, 2026 **Abstract:** Digital twins can provide vital insights into agricultural products and processes. There have been a lot of documented attempts at digital twins in agriculture. However, majority of these attempts build synthetic models and ignore the temporal dimension of the plant growth. Therefore, the existing models fail to depict actual plant details and growth. Our work replicates the actual growth of a real plant in the digital world by acquiring 3D meshes of the plant at various instants. It focuses on the transition between those acquired meshes by approximating all the consecutive pairs into approximate mesh pairs that have a common topology. The quality of these common approximate mesh pairs is quantitatively measured by an Energy term, which is minimized during the optimization process. Later, the meshes with the common topology are interpolated (morphing) to build the final digital twin of the plant. Experimental results show that the proposed methodology to attain the final morph has the potential to be a vital module, which could be responsible for the visual updates in the digital replica of the digital twin of the plant.
20.	Assessment of the correlation between macroscopic ICRS grading and histopathological OARSI scoring in osteoarthritic cartilage: An *Ex-Vivo* analysis **G Uppal,** T Goyal, A Kumar, R Sinha, M Kaur, **R Kumar** - Cartilage, 2026

	Abstract: Aims: Precise evaluation of cartilage damage is essential for the better management of osteoarthritis and treatment of articular cartilage. For accurate evaluation of cartilage damage, direct visual and/or histological assessment of articular cartilage is preferred over radiological or magnetic resonance imaging (MRI) imaging. This study aimed to determine whether, and to what extent, visual macroscopic grading using International Cartilage Repair Society (ICRS) system correlates with microscopic evaluation using the Osteoarthritis Research Society International (OARSI) histopathological scoring in an ex-vivo setting. Methods: A total of 70 articular cartilage sections obtained from 19 osteoarthritic human knees were macroscopically classified using the ICRS grading system and subsequently evaluated histologically using the OARSI scoring system. Spearman's correlation and bivariate linear regression analyses were performed to assess the association between ICRS and OARSI scores. The reproducibility, reliability, and inter- and intra-observer consistency of the OARSI scoring were further evaluated using Bland-Altman analysis, correlation coefficients, Cohen's kappa, Cronbach's alpha, and intraclass correlation coefficients (ICC). Results: Qualitative assessment revealed a progressive increase in OARSI histological scores corresponding to higher ICRS grades. Spearman's correlation and regression analyses demonstrated a weak positive correlation between visual ICRS grading and histological OARSI scoring in early-stage lesions (ICRS grades 0-I; $n = 29$, $r = 0.592$, $R^2 = 0.350$, $p < 0.001$), a moderate correlation with the inclusion of moderate-stage lesions (ICRS grades 0-II; $n = 47$, $r = 0.603$, $R^2 = 0.364$, $p < 0.001$), and a strong correlation when severely degenerated cartilage was included (ICRS grades 0-III; $n = 67$, $r = 0.811$, $R^2 = 0.657$, $P < 0.001$). The analysis of histological OARSI scores demonstrated narrow limits of agreement and minimal inter-observer variability in the Bland-Altman plot, excellent inter- and intra-observer agreement (ICC > 0.85), and almost perfect reliability (Cronbach's $\alpha > 0.95$). Conclusion: The results of the study demonstrated a stage-dependent association between macroscopic and histological assessments of osteoarthritic cartilage. The findings indicate that macroscopic ICRS grading may serve as a reliable tool for evaluating moderate to advanced stages of cartilage degeneration. However, its utility in early-stage lesions appears limited due to a weaker correlation with OARSI histological scores. Thus, while macroscopic visual evaluation should be interpreted with caution in early-stage degeneration, histological assessment using the OARSI scoring system remains a valuable tool for accurately identifying early degenerative changes.
21.	B-cell epitope prediction in the age of machine learning: advancements and challenges F Gabellieri, A Singh, **S Gupta**…R Mall - Journal of Translational Medicine, 2026 **Abstract:** Background: The identification of B-cell epitopes, the regions that bind to antibodies, is essential for creating effective prophylactic treatments against infectious diseases and cancer, particularly in the realm of reverse vaccinology. While experimental techniques like X-ray crystallography and peptide arrays help identify epitopes, they are expensive, time-consuming and differ in throughput and precision. Methods: This review examines how predictive techniques and datasets have evolved for the problem, highlighting recent breakthroughs in data-driven algorithms used to predict B-cell epitopes. We specifically examine how methodologies have progressed from traditional machine learning to cutting-edge deep learning models. Conclsion: The review summarizes significant research contributions in this domain including linear and conformational epitope prediction techniques, addresses methodological biases, dataset limitations, systematic evaluation challenges that plague the field, and explores future opportunities for innovation.
22.	Bypassing the synthesis bottleneck: A resource-stratified framework for advancing cancer drug discovery **DA Mosoh** - Medical Research Archives, 2026 Abstract: Despite the proliferation of validated oncogenic targets, the translation of bioactive natural products and high-throughput screening hits into clinical candidates is frequently stalled

	by the "Synthesis Bottleneck"—the prohibitive cost and technical difficulty of optimizing complex chemical scaffolds. This literature-based review addresses this critical impasse by proposing a paradigm shift from rigid structure-replication to function-mimicry, exemplified by the evolution of the complex marine natural product Halichondrin B to the simplified clinical drug Eribulin. It presents a resource-stratified framework that empowers researchers across the funding spectrum to navigate synthetic intractability. For resource-constrained academic laboratories, it highlights the emergence and revolution of ultra-large "make-on-demand" virtual libraries and pharmacophore hopping. For mid-tier biotechnology firms, it explores fragment-based drug discovery and free energy perturbation modeling to de-risk synthesis. For well-resourced pharmaceutical entities, it discusses the closed-loop integration of generative AI with autonomous robotic synthesis. Finally, it examines modality switching—specifically Proteolysis-Targeting Chimeras (PROTACs) and covalent inhibitors—as a strategic "escape hatch" for targets that remain refractory to traditional small-molecule optimization. By matching specific computational and experimental tools to available resources, this framework aims to democratize the discovery of developable cancer therapies and rescue promising biological hypotheses from the graveyard of intractable chemistry.
23.	Carbon nanodots as theranostics agents in cancer: Advances in design, targeting, and real-time monitoring **M Kumar, M Bhatt, B Das** - RSC advances, 2026 **Abstract:** Carbon nanodots (CNDs) have emerged as a promising class of carbon-based nanomaterials for cancer theranostics, uniquely integrating diagnosis and therapy on a single platform. Their ultrasmall size, high aqueous dispersibility, tunable photoluminescence extending into the near-infrared (NIR) window, and compatibility with green, scalable synthesis enable deep-tissue imaging and targeted intervention with reduced systemic toxicity compared with many conventional nanomaterials. This review summarises recent advances in the top-down and bottom-up fabrication of CNDs, including heteroatom doping and surface functionalisation with ligands or stimuli-responsive linkers, and relates these design parameters to optical performance, tumour selectivity, and responsiveness to the tumour microenvironment. Particular emphasis is placed on CND-based platforms for multimodal imaging (fluorescence, MRI, and photoacoustic), controlled-release drug delivery, gene silencing, and light-activated photodynamic and photothermal therapies, as well as emerging synergistic systems that combine these functions for real-time, image-guided treatment. Remaining challenges, such as batch-to-batch variability, incomplete understanding of long-term biosafety (especially for metal-doped CNDs), and limited clinical-scale manufacturing and regulatory readiness, are critically discussed alongside future opportunities, including NIR-II optimisation, protein-corona-resistant surface engineering, and AI-assisted CND design for personalised cancer theranostics.
24.	Characterisation of drek wood, jackfruit and pineapple peels for thermochemical conversion **M Mustapha, I Dhada, R Das,** AK Shukla - Results in Engineering, 2026 **Abstract:** Biomass thermochemical conversion is a cost-effective and eco-friendly alternative energy source. This study evaluates the potential of drek wood (DW), pineapple peel (PP), and jackfruit peel (JP) as viable feedstocks for gasification. Various characterisation was performed, including proximate and ultimate analyses, alongside FESEM-EDX, FTIR, XRD, and TGA-DTA, to assess their bioenergy properties. The results show that DW, JP, and PP possess low moisture (6.24-7.25%) and ash contents (1.74-7.02%), with high volatile matter (75.75%-80.44%). DW possesses the lowest ash content (1.74%) and exhibits the highest heating value (18.19 MJ/kg). FTIR, FESEM, and XRD analysis confirmed the materials showed a typical lignocellulosic behaviour, identifying key functional groups (C-O, C-H, C=C, and O–H) and structural components (cellulose, hemicellulose, lignin). EDX ash analysis revealed a significant presence

	of alkali and alkaline earth metals, which are known to enhance syngas heating value, reactivity, and carbon conversion efficiency. The thermal analysis showed a lower ignition temperature for PP (175°C) and JP (208°C), indicating their higher reactivity and ease of combustion. The PP DTA curve further exhibited several exothermic peaks across 214°C-331°C due to its reactivity. Meanwhile, DW experienced the greatest mass loss during the devolatilization stage (58.88%), indicating high cellulose content. Overall, these findings emphasise the impressive gasification potential of DW and the valorisation of JP and PP waste as renewable resources. 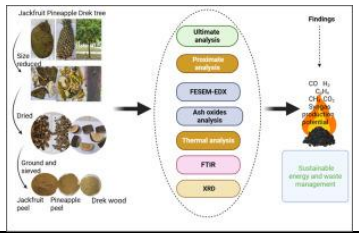
25.	Collisional dynamics of NC_4NH^+ with H_2 in the interstellar medium **P Chahal, TJD Kumar** - Monthly Notices of the Royal Astronomical Society, 2026 **Abstract:** The present work explores the quantum dynamics of protonated dicyanoacetylene (NC_4NH^+) in collision with both para and ortho-H_2 over the temperature range 1–100K. Such low-temperature collisions help determine the state-to-state rate coefficients for the rotational transitions of NC_4NH^+, a recently detected species in TMC-1. To study these collisions, a four-dimensional (4D) ab initio potential energy surface (PES) for the NC_4NH^+–H_2 system was developed using the CCSD(T)–F12b method with an augmented correlation consistent polarized triple-zeta basis set under the rigid-rotor approximation. The PES was then augmented through a neural network (NN) fitting approach to get the dense data. It was further expanded in bispherical harmonics, for the radial coefficients to be expressed in analytical form. Based on these radial coefficients, state-to-state cross-sections and rate coefficients were calculated using the exact close-coupling method for the rotational states considering to both para and ortho-H_2. For rate coefficients it is observed that a strong propensity is favored for even transitions over the odd ones. The resulting rate coefficients would also help model the abundance of NC_4NH^+ in the interstellar medium under non - local thermodynamic equilibrium conditions.
26.	Comparative study on high-temperature isothermal oxidation behavior of cold spray additively manufactured (CSAM) hastelloy-X and inconel 718 superalloy thick deposits **S Singh, A Anupam, H Singh** - Progress in Additive Manufacturing, 2026 **Abstract:** High-temperature oxidation resistance ensures the lifetime and performance of nickel-based superalloy components operating at high temperatures. Hastelloy X (Hast-X), a solid solution-strengthened nickel-based superalloy, is known for its superior mechanical qualities and resistance to high-temperature oxidation. In some sophisticated industrial applications, these properties make it a possible alternative to the commonly used nickel-based superalloy, Inconel 718 (IN718). This study compares the isothermal oxidation behavior of Hast-X and IN718 thick deposits, which are deposited via a cold spray additive manufacturing process (CSAM). Isothermal oxidation tests conducted at 1100 °C for up to 100 h revealed that the oxidation kinetics curves of both as-deposited superalloys adhered to the parabolic law. The oxide scales primarily consisted of granular Cr_2O_3 and outer spinel layers of $NiCr_2O_4$, $NiFe_2O_4$, Fe_2O_3, and $FeCr_2O_3$. Additionally, Al_2O_3 was detected in the oxidized IN718 samples. Despite the finer Cr_2O_3 grains in IN718, its oxide scales exhibited severe spallation at elevated temperatures. Hast-X has better high-temperature oxidation resistance, which could be attributed to the uniformly distributed dense Cr_2O_3 and relatively slight exfoliation of oxides in the oxide scales.
27.	Confining polyiodide in polymer cathode boosts cycling stability in high energy-dense aqueous zinc-sulfur batteries

	TS Thomas, AP Sinha, D Mandal - Small, 2026 **Abstract:** Aqueous zinc-sulfur (Zn/S) batteries are emerging as sustainable energy storage systems owing to their high theoretical capacity, environmental safety, and cost-effectiveness. However, their practical application is hindered by sluggish solid-solid sulfur conversion kinetics and the persistent need for soluble iodine redox mediators that exacerbate zinc anode corrosion and dendrite formation. Here, we report an integrated polymer–polyiodide confinement strategy employing a cationic poly(vinyl butyl imidazolium iodide) framework ([PVIM]I) complexed with iodine to form a redox-active polymer-polyiodide framework ([PVIM]I_x). The polymer matrix spatially confines polyiodide species, minimizing their crossover and suppressing zinc anode corrosion while enhancing sulfur redox kinetics. The resulting metal-free and binder-free ([PVIM]I_x) cathode delivers a high specific capacity of 1845 mAh g^{-1} (1548 mAh g^{-1} excluding iodine contribution) at 0.1 A g^{-1} with an energy density of 923 Wh kg^{-1}, maintaining excellent cycling stability with 93.7% capacity retention over 500 cycles at 5 A g^{-1}. Improved ion diffusion and reduced polarization were confirmed by GITT and in situ impedance spectroscopy. This polymer-iodide composite provides a scalable and stable platform for advancing aqueous Zn/S batteries, addressing key challenges in cathode wettability and redox mediation to enable sustainable, high-performance energy storage solutions.
28.	Controlling quasiparticle population dynamics in WS_2 monolayer using optical pumping NK Mishra, **Swetha K,** A Sharma, V Balakrishnan, **RV Nair,** J George - Advanced Optical Materials, 2026 **Abstract:** Controlling the quasiparticle population density in 2D materials is crucial for designing next-generation devices. In this study, we explore how optical pumping effectively controls the population and dynamics of quasiparticles (excitons, trions, and biexcitons) in exfoliated and CVD-grown WS_2 monolayers at room temperature. Photoluminescence analysis reveals that the emission profile primarily consists of excitons and trions in the low-pump power regime. The densities of the unbound electrons follow the law of mass action, and the trion population increases with increasing pump power. Furthermore, the excitation-energy-dependent conversion efficiency is systematically investigated and found to be consistent with pump energy. In the high-power regime, photoluminescence spectra reveal the formation of biexcitons and defect states, as confirmed by Raman measurements. Additionally, lifetime measurements are performed to assess variations in the radiative and non-radiative contributions by varying the pump power, which are correlated with steady-state measurements. Spectral diffusion and bleaching experiments reveal a higher purity of the exfoliated monolayer compared to the CVD-grown samples. These findings are crucial for designing high-performing 2D material-based devices.
29.	Copper-catalyzed intramolecular carbocyclization/1, 2-migration reaction of allenols to access substituted 2-sulfonyl carbazoles **P Singh, P Nain,** MV Mane, **AC Shaikh** - Organic Letters, 2026 Abstract: A copper-catalyzed intramolecular cascade carbocyclization/1,2-migration of C-2 indolyl-allenol has been achieved to construct the library of 2-sulfonyl carbazoles, which possess considerable biological significance. This modular protocol is operationally simple, exhibiting a broad substrate scope with consistently high yields. Additionally, gram-scale synthesis, product diversification of 2-sulfonyl carbazoles, and DFT studies of the catalytic cycle have been performed. Overall, this study unfolds a new strategy for the one-pot synthesis of sulfonyl carbazoles, which holds significance in medicinal and material chemistry.

	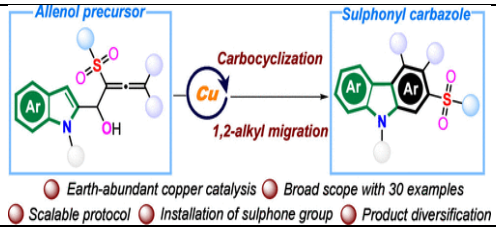
30.	Deep eutectic solvent–mediated solubilization enhancement of quercetin: Experimental, molecular dynamics, and biological evaluation Y Vora, **M Prajapati, K Bhavya, D Pal, K Kumar,** K Kuperkar - Journal of Molecular Liquids, 2026 **Abstract:** Deep eutectic solvents (DESs) have recently gained significant attention across various scientific and technological fields. As interest in DESs continues to grow, understanding their impact on drug solubility is crucial for developing better drug formulations. Our study provides a detailed investigation of the interactions and the biological behaviour of DES composed of choline chloride (ChCl) and levulinic acid (Lev) in the molar ratio 1:2, with the quercetin (QCT). To validate the preparation of ChCl: Lev, we measured its physicochemical properties, spectroscopic properties, and thermal analysis. Here, we investigated the solubility of QCT in ChCl: Lev by UV-Vis spectroscopy at ambient conditions, which revealed that the QCT in ChCl: Lev increased by approximately 70,000 times compared to pure water. Therefore, ChCl: Lev shows potential as an effective carrier for enhancing the bioavailability of poorly soluble compounds in preclinical studies. Also, the COSMO-RS approach was used to screen the HBA and HBD combination by calculating the sigma- (σ) profile and predicting the solubility of the QCT in ChCl: Lev at a temperature range. Furthermore, MD simulations were performed to investigate the structural and dynamic properties of ChCl: Lev in the presence of QCT. The simulations analyzed interaction energies between components and examined structural properties, including atom-atom radial distribution function (RDF), mean squared displacement (MSD), and the hydrogen bonding network, providing insights into the effective interactions of QCT within ChCl: Lev. Compared to conventional solvents such as DMSO, ChCl: Lev offers superior quercetin solubilization while preserving hemocompatibility and cellular safety. Moreover, the biological performance of quercetin in ChCl: Lev (QCT-ChCl: Lev) was evaluated through antibacterial activity, cytotoxicity, and hemocompatibility assays. Collectively, these results suggest that while ChCl: Lev is highly effective in enhancing quercetin solubility and antibacterial activity, the associated cytotoxicity toward normal fibroblast cells highlights a concentration and cell-type-dependent toxicity profile, necessitating cautious interpretation and further optimization before broader biomedical application. 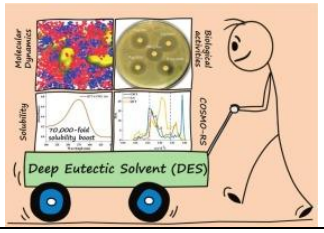
31.	Developing effective water policies for dairy farms in Punjab: A focus on seasonal and species-specific requirements **H Sharma,** I Kaur, PK Singh - Indian Journal of Economics and Development, 2025 **Abstract:** The present study was conducted on 180 crossbred cows, 447 buffaloes and 196 indigenous cattle across the state of Punjab to address this issue. The analysis yielded several noteworthy findings regarding water consumption and footprint in dairy farming systems, particularly in Punjab, India. From the selected farms, data on water usage in milk production were

	collated on a seasonal basis. On average, farms consumed 8.43 litres of water per kg of FPCM. Indigenous cattle generally exhibited higher water footprints per kilogram of FPCM produced, with crossbred cattle having the lowest footprint. The study also highlighted the broader impact of dairy farming on water resources, particularly in Punjab, where groundwater depletion poses significant challenges. Despite dairy farming's considerable water footprint, it was found to be lower than that of other agricultural activities, such as rice cultivation. Overall, the results underscore the importance of adopting sustainable water management practices in dairy farming to mitigate environmental impacts and ensure long-term sustainability, particularly in regions facing water scarcity, such as Punjab.
32.	Effect of Ce concentration on the oxidation behavior of β-NiAl alloy **S Kumar, PK Ray** - Journal of Materials Engineering and Performance, 2026 **Abstract:** The effect of varying Ce concentration (1.0 at.% & 0.1 at.%) on oxidation behavior of β-NiAl alloy is investigated at 1100 °C using x-ray diffraction, scanning electron microscopy and x-ray spectroscopy techniques. Oxidation experiments are conducted in two stages: (1) A series of ex situ transient-oxidation experiments are performed to observe the dynamic changes during initial 10 hours of oxidation, (2) long-term oxidation experiments (100 hours) are performed to reveal the oxide surface and cross section morphology. Further, the dynamic effects are then compared to explain oxide growth kinetics, which invariably change the scale thickness and the oxidation behavior. We observed that the reduction in Ce concentration from 1.0 at.% to 0.1 at.% results in a significant reduction in oxide growth rate. After 100 hours of oxidation, a needle shaped Al_2O_3 morphology is observed at the surface. Oxide cross section micrographs reveal that the phenomenon of internal oxidation occurs simultaneously along with external oxidation. However, the propagation of the internal oxidation front is slower at low Ce concentration, resulting in slower oxide growth and a relatively planar scale. Our work explains the efficacy of low Ce concentration on the quantitative improvement in oxide growth kinetics, offering alloy design principles for RE-doped β-NiAl-based oxidation-resistant alloys.
33.	Effect of particle shape and addition of oppositely charged particles with different wettability on droplet bridging M Tiwari, J Padhi, **M Sabapathy,** VR Dugyala - The Journal of Chemical Physics, 2026 **Abstract:** This work demonstrates the effect of a heterogeneous mixture of oppositely charged particles with different shapes and wettability on the stability of droplet bridging. For this purpose, micron-sized hydrophilic hematite particles with ellipsoidal, spherocylindrical, cubic, and dumbbell shapes are employed as emulsifiers. To prepare the emulsions, these particles are modified *in situ* with oleic acid in an immiscible water–decane system. The results confirm that droplet bridging is controlled by tuning the particle wettability and adhesive force alone while the required oleic acid concentration range for droplet bridging and the resulting two-dimensional (2D) particle arrangement at the bridge depend on the particle shape. Ellipsoids and spherocylinders form short chains with random orientation in a side-by-side arrangement, whereas cubes and dumbbells arrange into long-range 2D crystal structures with square and triangular lattices, respectively. Moreover, the effect of adding oppositely charged particles with different wettability (hydrophobic polystyrene and hydrophilic silica particles) to the hematite particles on droplet bridging and particle ordering is also investigated. When the amount of hydrophobic particles added to the hematite system exceeds a critical ratio, the system transitions from bridged emulsions to individual droplets. Increasing the number of hydrophobic particles destabilizes bridging by causing the bridged interfaces to merge whereas adding hydrophilic particles promotes stable bridged emulsions by remaining within the hematite bridge without merging the interfaces. This approach enables the design of 2D ordered crystals of binary particles at the droplet bridge.

	Notably, this study demonstrates that oppositely charged particles can be used to tune and stabilize bridged emulsions under optimal conditions.
34.	Engineering Cu catalysts on metal-modified mesoporous silica supports from rice husk ash for selective furfural hydrogenation **A Jaswal, V Garule, T Mondal** - Biomass Conversion and Biorefinery, 2026 **Abstract:** This study investigates the catalytic performance of low loading Cu catalysts supported on rice husk-ash derived mesoporous silica support modified with metals (Al, Sn, Ti and Zr) for the vapor-phase hydrogenation of FFR to FAL. The catalysts underwent thorough characterization employing XRD, H_2-TPR, NH_3-TPD, FTIR, N_2 physisorption, XPS, and FESEM techniques, providing comprehensive insights into their properties. The analyses revealed significant structural modifications in the silica framework upon metal modification. XRD and N_2 physisorption analyses indicated the disruption of the mesoporous structure, accompanied by a reduction in surface area and pore volume. FTIR and XPS confirmed metal integration into the silica framework, improving the reducibility of the supported CuO species, as evidenced by H_2-TPR as well as improving the acidic site strength, as seen from NH_3-TPD. Further analysis through Auger spectroscopy revealed the dominance of Cu^+ species in the catalysts with metal-incorporated silica support. The changes induced by metal modification became apparent during catalytic activity assessment where the incorporation of metals yielded increased FFR conversion and FAL yield over pure mesoporous supported catalyst. Zr-incorporated Catalyst (Cu@Zr-MS) yielded the most favourable outcomes among all catalysts, due to a combination of adequate acidic sites of appropriate strength, synergy between Cu^0 and Cu^+ species, the presence of oxygen vacancies and oxophilicity conferred by Zr. Optimization of process parameters revealed peak FFR conversion and FAL yield over Cu@Zr-MS at H_2/FFR = 10, Temperature = 200 °C, and WHSV = 1 g_{FFR} h^{-1} $g_{catalyst}^{-1}$, with respective values of 90.6% and 85% despite a small Cu loading. Assessment of catalytic performance over prolonged reaction duration demonstrated stable conversion at around 90%, alongside a sustained FAL yield of ~ 85% over approximately 16 h before a decline set in, with progressive deactivation that can be ascribed to sintering of Cu^0 particles as well as the formation of amorphous carbonaceous species on the surface and/or inside catalyst's pores. 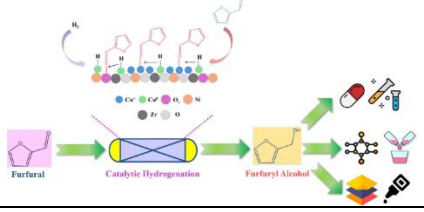
35.	Estimating the location of sheath-to-ground faults occurring at any distance away from joints in cross-bonded cables in online condition **A Das, CC Reddy** - IEEE Transactions on Dielectrics and Electrical Insulation, 2026 **Abstract:** Locating sheath-to-ground faults in cross-bonded power cables is challenging, particularly when faults occur away from joint locations. Most existing techniques are limited to joint-based fault assumptions and require measurements from multiple links and grounding boxes, which restricts their practical applicability. This paper proposes an online method for estimating the location of sheath to ground faults at arbitrary positions along cross-bonded cables using only sheath earthing currents measured at grounding boxes. A comprehensive circuit model incorporating the mutual coupling between conductors and sheaths of all phases, including cross-bonding effects, is developed. Based on this model, an analytical expression for SGF location estimation is derived. The proposed method is validated through laboratory experiments, circuit simulations, and field measurements on a 220 kV transmission cable system, demonstrating accurate fault location without the need for link-box current measurements.

36.	Exceptional point driven by asymmetry in meta-resonators in a non-Hermitian complementary terahertz metasurface A Bhardwaj, M Islam, C Kumar, A Panwar, **G Kumar** - Journal of Applied Physics, 2026 **Abstract:** In this paper, we investigate a non-Hermitian open terahertz metasurface comprising complementary structures capable of exhibiting parity-time symmetry. The metasurface consists of two asymmetric resonators of different sizes, representing effective gain and loss elements, placed orthogonally in a strongly coupled near-field configuration. When one resonator is displaced diagonally with respect to the other, the exceptional point appears where the system undergoes a phase transition from a PT-symmetric to a PT-asymmetric state. We fabricate the samples in a clean room ambience to experimentally validate the exceptional points. Terahertz time-domain spectroscopy is performed on the fabricated samples to experimentally corroborate the transmission properties observed in numerical simulations. We further employ coupled mode theory to analyze and distinguish between the PT-symmetric state, exceptional point, and PT-asymmetric state. Theoretical framework enables the calculation of eigenvalues, phase spectra, and eigenmodes associated with the metamaterial design, thereby again corroborating the simulation results. Furthermore, we construct the Poincaré sphere to visualize the orientation of the polarization states of the eigenmodes, which again suggest the presence of an exceptional point. The study holds potential to develop highly sensitive terahertz devices, addressing limitations of conventional PT-symmetric systems that rely on traditional gain and loss media.
37.	Experimental investigation of multi-strain bacterial concrete: Self-healing efficiency, strength, and sorptivity under varied curing conditions RB Singh, A Kumar, D Sharma, **SK Sahdeo** - Journal of Building Engineering, 2026 **Abstract:** Concrete despite being the cornerstone of modern infrastructure has the tendency to crack because of its brittleness. In recent years, researchers have tried to reduce such issues by investigating microbial solutions. This research addresses one possible way of introducing bacterial strains into the concrete matrix, to remain dormant until the water penetrates the matrix. The bacteria (if activated) break-down calcium lactate and form calcium carbonate ($CaCO_3$) which closes the cracks and makes the material more robust. In the present study, three bacterial isolates *Escherichia coli*, *Bacillus subtilis* and *Streptomyces toxytricini* were included into M25 grade concrete. Calcium lactate 5% was used as a constant nutrient source and different dosages of 3% and 6% (by cement weight) were tested. In addition, standardized mixing, casting, and curing procedures were adhered to. The study was conducted for determining the self-healing effectiveness, compressive strength and sorptivity with different curing regimes. The results demonstrated significant crack-healing ranged from approximately 89% to 97% after 28 days, depending on type of bacteria and curing. The highest compressive strength of 40 MPa was achieved with 6% *Streptomyces toxytricini* bacteria that showed an increase of 79% compared to controlled concrete. The lowest sorptivity value of 0.0007 $mm/s^{1/2}$ was obtained for concrete containing 6% *Streptomyces toxytricini* that indicated improved resistance to long-term moisture ingress. The results showed that the addition of bacteria provided crack healing, enhanced compressive strength and significantly influenced the moisture absorption properties, thus showing the potential of bacterial concrete as a sustainable construction material.
38.	First-principles insights in designing two-dimensional by$Y_{1-x}Z_x$ (Y, Z = P, As, and Sb, but Y ≠ Z) alloys: A potential candidate for thin-film optoelectronic devices DK Sharma, P Kumar, **R Ahuja,** S Kumar - The Journal of Physical Chemistry C, 2026 **Abstract:** Forming two-dimensional (2D) alloys provides a unique way to tune the structural parameter and the electronic structure of a material in comparison to their pure counterparts. By taking motivation from this fact, we are presenting a detailed analysis based on first-principles

	density functional theory calculation for 2D $BY_{1-x}Z_x$ (Y, Z = P, As, and Sb, but Y ≠ Z) alloys. From a synthesis point of view, it would be interesting to predict (*a*) How the structural parameters and electronic structure of $BY_{1-x}Z_x$ alloys are going to change with doping concentration (*x*)? (*b*) How will *x* affect the thermodynamical stability of alloys? and (*c*) What are the growth temperatures of these alloys? Our calculations reveal that an increase in *x* decreases the lattice constant of $BY_{1-x}Z_x$ alloys, which is in accordance with Vegard's law. Electronic structure calculations predict a direct band gap for pristine BP, BAs, and BSb at high symmetry point *K*, equal to 1.35, 1.18, and 0.60 eV, respectively. We notice that for $BY_{1-x}Z_x$ alloys, the band gap remains direct and shows bowing at $x = 0.33$. There is a sharp fluctuation in edge valence bands during the band alignment of alloys (maximum for $BSb_{1-x}As_x$, ~1 eV). However, the edge conduction bands show a relatively small fluctuation, which is the lowest for $BAs_{1-x}P_x$ alloys (~0.02 eV) on increasing *x*. The absorption coefficient of $BY_{1-x}Z_x$ alloys as a function of *x* shifts the peak toward blue. Further, $BAs_{1-x}P_x$ alloys exhibit positive enthalpy of mixing and thus can grow by obeying an endothermic reaction. However, $BSb_{1-x}P_x$ and $BSb_{1-x}As_x$ alloys, with negative mixing enthalpies, can be grown by an exothermic reaction. The binodal and spinodal decomposition curves predict the growth temperature of $BAs_{1-x}P_x$, $BSb_{1-x}P_x$, and $BSb_{1-x}As_x$ alloys to be −208, 3082, and 1801 K, respectively. 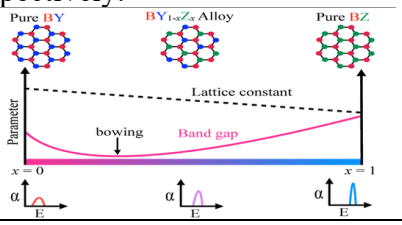
39.	Flexible MoS-based ion-selective sensor with valinomycin membrane for in-situ detection of soil potassium (K+) ions **P Shukla, R Gond, B Rawat** - IEEE Sensors Letters, 2026 **Abstract:** In this letter, we report the flexible MoS_2/valinomycin-based sensor for in situ K^+ detection in the soil sample. The fabricated sensor, realized on a flexible PET substrate using scalable ink-dispensing techniques, exhibits a wide detection range of 1–100 mM with high linearity ($R^2 = 0.9975$) and sensitivities of 5.6 µA/mM in analyte solution and 2.1 µA/mM in soil sample. More importantly, cyclic voltammetry analysis reveals stable and reversible oxidation–reduction behavior across repeated cycles, with excellent reproducibility in multiple sensor replicas. The fabricated sensor uniquely combines soil compatibility, flexibility, reproducibility, and cost-effective fabrication, which addresses the critical gap between laboratory sensing technologies and field-deployable soil nutrient monitoring. These results establish the MoS_2/valinomycin sensor as a robust and scalable platform for precision agriculture, with the potential to advance real-time nutrient management and promote sustainable farming practices. 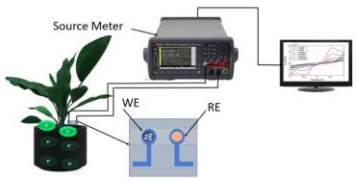
40.	Formulation of a transformation-based approach to regional flood frequency analysis in LH-moment framework **AK Singh, SR Chavan** - Journal of Hydrology, 2025 **Abstract:** Regional flood frequency analysis (RFFA) facilitates the estimation of design floods at ungauged locations within hydrologically homogeneous regions. The utilization of higher order L-moments, famously known as LH-moments has proven to be more effective and advantageous

	in quantifying the design floods, particularly corresponding to larger return periods. In this paper, a transformation-based RFFA approach is formulated in LH-moment framework, considering five widely recognized peak flow distributions, namely Generalized Extreme Value, Generalized Logistic, Generalized Pareto, Pearson Type III and Generalized Normal distributions. Further, the expressions for location, scale and the shape parameters of Pearson Type III, Generalized Normal and Kappa distributions are derived using LH-moments in original space, since their unavailability. A Monte Carlo simulation experiment has revealed better performance of the formulated approach relative to conventional RFFA approach as well as L-moment based transformation approach. Finally, the efficacy of the developed transformation-based approach is validated through applications to real world catchments of the conterminous United States, and four major river basins in South India. Results indicate that the transformation-based approach to RFFA tend to outperform the conventional RFFA approach in LH-moment framework. The proposed approach offers substantial improvement in the accuracy of design flood estimates for large return periods in ungauged or data-scarce catchments, making it a reliable tool for analyzing highly skewed flood datasets.
41.	Fusion of 9Be with 116Sn at near-barrier energies **N Garg, R Kaur, Priyanka, S Devi, K Tiwari, S Thakur**…**PP Singh** - Physical Review C, 2026 **Abstract:** In this study, fusion cross sections for the 9Be+116Sn reaction have been measured at near-barrier energies, within the range of 0.75 Vb < Elab(MeV) <1.16 Vb. This investigation aims to explore the influence of the intrinsic structure of the 9Be projectile on fusion dynamics. The experimentally measured fusion excitation functions have been analyzed and interpreted using the coupled-channel approach using the ccfull code, which includes couplings to the collective excitations of both the projectile and target nuclei. While these calculations adequately describe sub-barrier fusion, they indicate a significant suppression of fusion (approximately 35%) at above-barrier energies, suggesting the impact of noncollective effects, such as projectile breakup. The barrier height, determined from the analysis of the barrier distribution, is found to be ≈26.11±0.30 MeV. The reduced excitation functions of the 9Be+116Sn system have been contrasted with those involving more tightly bound projectiles, such as 16,18O and 32S. It has been observed that 9Be exhibits the highest enhancement in sub-barrier fusion and a considerable suppression at above-barrier energies. This highlights the dependence on projectile structure, particularly given the low breakup threshold of 9Be. Furthermore, the systematic behavior of fusion suppression involving the 9Be projectile with various targets, 9Be+x, has also been investigated by applying the universal fusion function and the improved fusion function to the experimentally measured excitation functions. The results of this study indicate that the target nuclei have minimal to no influence on the observed fusion suppression.
42.	Generating nondiffracting bottle beams with a flat multilevel diffractive lens AN Kumar Reddy… **V Pal**… T Omatsu - ACS Photonics, 2026 **Abstract:** We introduce a novel method for generating a high-quality, sharply defined, nondiffracting optical bottle beam by focusing a Bessel beam propagating through a flat multilevel diffractive lens (MDL). This study highlights the impact of the MDL illuminated by a Bessel beam with suppressed sidelobes generated from a binary axicon. The resulting Bessel bottle beam exhibits a series of low- or zero-intensity zones interleaved with high-intensity regions, with periods ranging from 0.2 to 1.36 mm along the beam propagation direction. The transverse intensity profiles of these regions remain shape-invariant over long distances in free space, and thereby, the nondiffracting range of the micron-sized optical bottle beam exceeds 5 cm. We also observe that the far-field output from the MDL, when illuminated by a Bessel beam, offers advantages over that of conventional focusing lenses. Furthermore, this technique can operate on ultrafast time scales (from pico- to femtoseconds) due to the high damage thresholds of the binary

	axicon and MDL, enabling the generation of high-power optical bottle beams. Ultimately, our experimental approach paves the way for various applications, including high-resolution biological imaging in turbid media, particle manipulation, micromachining, and harmonic generation, by leveraging the spatial landscape of the optical bottle beam. 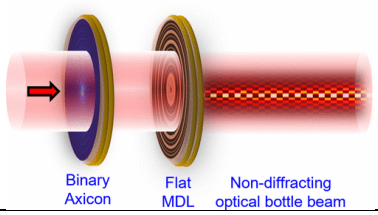
43.	High-order harmonics generation in MoS2 nanosheets in the presence of CdSe and CdSe/V2O5 quantum dots **SR Konda,** P Barik, **S Kumari,** S Singh… Wei Li - Applied Physics Letters, 2026 **Abstract:** Engineering nonlinear optical responses in two-dimensional materials via heterostructure design is emerging as a powerful approach for next-generation photonic devices. Although perturbative nonlinear effects in these systems are well studied, their connection to nonperturbative processes such as high-harmonic generation (HHG) remains largely unexplored. Here, we investigate the HHG from few-layer MoS_2 nanosheets integrated with CdSe and passivated $CdSe/V_2O_5$ quantum dots (QDs). The hybrid structures exhibit pronounced enhancement in harmonic intensity and a clear extension of the harmonic cutoff relative to pristine MoS_2. We demonstrate that interfacial charge-transfer dynamics—previously associated with the dominant contribution to the third-order susceptibility $\chi^{(3)}$—also govern the efficiency of HHG, thereby establishing a direct link between perturbative and nonperturbative regimes in these 0D–2D hybrids. The carrier injection from the QDs increases the electron–hole population participating in HHG, while the moderated response in passivated QD systems highlights the role of interfacial potential barriers. These results provide a unified physical picture of nonlinear optical processes in hybrid nanostructures and offer design principles for enhancing coherent light generation.
44.	Innovative hybrid approach for clean, battery-free fuel cell vehicles with optimized DC-DC conversion RG Bodkhe, **PK Pandey,** A Agrawal… - Environment, Development and Sustainability, 2026 **Abstract:** Energy management in fuel cell vehicles (FCVs) remains a major challenge, affecting hydrogen utilization, system lifespan, and overall efficiency. Traditional FCVs require additional batteries or ultra-capacitors to stabilize voltage during dynamic load conditions, which increases cost and environmental burden. This study aims to evaluate a battery-free FCV architecture that eliminates the need for auxiliary energy storage by optimizing DC-DC converter and integrating energy management to improve voltage regulation, reduce system cost, and enhance hydrogen utilization. The proposed system integrates a DC-DC converter, whose control factors are optimized utilizing Gazelle Optimization Algorithm (GOA) to achieve cost minimization and voltage stability. A Hybrid Graph Convolutional Neural Network (HGCNN) is also employed to enhance predictive energy management, improving hydrogen economy and extending fuel cell life. This combined approach is named as GOA-HGCNN. The approach is simulated using MATLAB and findings demonstrate that proposed GOA-HGCNN technique achieves substantial reduction in FC cost compared to various existing methods. The method also ensures stable voltage regulation under varying operating conditions, reduces torque ripple and improves efficiency without requiring lithium-ion batteries or super capacitors. The proposed GOA-HGCNN hybrid control strategy delivers a scalable, cost-effective, and sustainable solution for battery-free FCVs. By eliminating battery dependency and enhancing hydrogen utilization, the study supports long-

	term system reliability, reduced environmental impact, and alignment with clean mobility objectives.
45.	In-situ ammonia synthesis and energy generation via aqueous Zn-NO3-battery **A Chaturvedi, S Mehta, TC Nagaiah** - Journal of Materials Chemistry A, 2026 **Abstract:** The sustainable generation of electricity and ammonia (NH_3) is essential for modern industrial advancement. The electrochemical nitrate reduction reaction (NO_3RR) provides a sustainable pathway for NH_3 production, complemented by pollution mitigation. Nevertheless, this process is constrained by limited nitrate adsorption, multiple competing reactions, and sluggish kinetics involving coupled proton–electron transfer steps, thereby reducing NH_3 selectivity. Herein, we have utilised FeCu(1:2)S_x as a cathode catalyst in Zn–NO_3^- battery to produce NH_3 *via* the NO_3RR, simultaneously generating electricity. The assembled Zn–NO_3^- battery demonstrated a remarkable faradaic efficiency (F.E.) of 98.96% for NH_3 and a power density of 5.2 mW cm^{-2}. Real time NH_3 production examined by *in situ* electrochemical Raman and attenuated total reflectance-Fourier transform infrared (ATR FT-IR) spectroscopy revealed that Cu promotes NO_3^- adsorption and reduction to NO_2^-, while Fe facilitates hydrogenation resulting in an NH_3 yield of 3.69 mg h^{-1} cm^{-2} at −0.9 V *vs.* RHE. As a proof of concept, two Zn–NO_3^- batteries connected in series powered 62 LEDs for over 70 h.
46.	Interfacial atomic configuration dependent thermoelectric properties in graphene-hBN heterostructures **Renu, R Kumar** - Surfaces and Interfaces, 2026 **Abstract:** Interfaces in two-dimensional heterostructures significantly influence their electronic properties. However, the effect of interfacial atomic configurations on thermoelectric properties has remained overlooked. In this study, we investigate the electronic and the thermoelectric properties of Graphene-hBN heterostructures by varying the interfacial atomic configurations using first-principles calculations. It is noted that interfacial atomic configurations and the van der Waals (vdW) interactions strongly modulate the electronic as well as the phononic responses, directly influencing transport properties. The results shows that the configuration with the maximum vdW interaction has the maximum charge redistribution and phonon scattering at the interfaces, leading to the maximum ZT value. However, variations in interfacial atomic arrangement with similar vdW interactions lead to different ZT values. These findings provide valuable insights for designing interfacial atomic configuration dependent heterostructures for advanced electronic and thermoelectric applications. 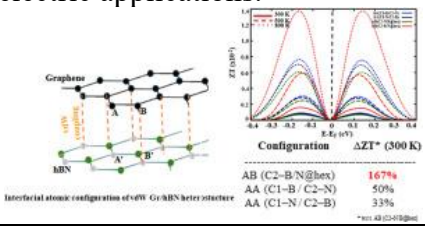
47.	Late amazonian glaciation in the acheron fossae region of mars **T Ghosh, RK Tiwari,** RK Sinha, RR Bharti - Advances in Space Research, 2025 Abstract: The Acheron Fossae region in the Martian mid-latitudes (31.5° N, 143.2° W–40.5° N, 129.2° W) preserves a diverse assemblage of ice-related landforms, offering key insights into the nature and timing of Late Amazonian glaciation. This study presents the comprehensive glacial history of the region, using topographic, image, and SHARAD radar data. Our detailed geomorphic mapping of glacial landforms revealed extensive lobate debris apron (LDA) and lineated valley fill (LVF) systems exhibiting flow lineations terminating in lobate and piedmont-like forms, along with concentric crater fill (CCF) and small-scale LDAs marking localized ice accumulation in the

	region. Flow patterns show compression, bending, wrapping, and funneling around topographic obstacles, while surface textures including ridge-and-furrow patterns, isolated knobs, pits, rimmed depressions, polygonal cracks, ring-mold craters, and brain-terrain, suggest progressive degradation of glacial landforms. Crater size–frequency distribution (CSFD) analyses yield model ages of ~150 ± 5 Ma for the main LDA/LVF systems and ~42 ± 3 Ma for small-scale LDAs, implying episodic glacial phases in the Late Amazonian. Synglacial craters indicate alternating epochs of impact cratering and glacial modification temporally and potential ghost LDA (GLDA) depressions resulting from lave-ice interactions suggest an even longer glaciation, extending back to ~1 Ga. SHARAD radar data indicate absence of subsurface reflections, implying that ice is either absent, or buried beneath mantling deposits. Morphologically distinct channel types are evident in the region, with one potential esker-like ridge, implying localized events of glacial ice melting. Altogether, the suite of geomorphic features, stratigraphic, and age relationships reveal that Acheron Fossae experienced prolonged and episodic glaciation.
48.	Lebesgue differentiation theorem with uncentered balls on metric spaces **MA Bhat, GSR Kosuru** - The Journal of Analysis, 2026 Abstract: We prove a version of the Lebesgue differentiation theorem for uncentered averages in general metric measure spaces under suitable localized volume growth conditions.
49.	LH-moment framework for regional flood frequency analysis based on Log-Pearson Type III distribution **AK Singh, SR Chavan** - Hydrological Sciences Journal, 2026 **Abstract:** Efficacy of Log-Pearson Type III (LPIII) distribution to perform regional flood frequency analysis (RFFA) in the LH-moment framework is explored in this paper, especially when the peak flow datasets exhibit high skewness. The formulations for parameter estimation of the LPIII distribution are derived in the LH-moment framework. Further, the effectiveness of LPIII distribution in predicting the design flood estimates at ungauged locations is assessed through Monte Carlo simulation experiments. The relative performance of the LPIII distribution in ungauged predictions with reference to other skewed peak flow distributions is examined by performing Leave-One-Out Cross Validation. Results indicate better performance of LPIII distribution over the skewed distributions, especially when the return periods are greater than 75 years. The utility of the approach is tested through case studies on South India and the conterminous United States. Overall, it is inferred that LPIII distribution can be considered as a regional distribution for the reliable prediction of design floods.
50.	Low vowel raising in Malayalam **AR Jacob, S Kar** - SN Social Sciences, 2026 **Abstract:** The Dravidian language Malayalam exhibits a range of vowel-related phonological processes, including vowel reduction, deletion, lengthening, sandhi, schwa insertion and glide formation. The synchronic phonological process of Low Vowel Raising (LVR) is observed in Malayalam, which occurs exclusively in borrowed words and not in core Dravidian lexicons—the low vowel raises to a mid-high vowel when the preceding consonant is a voiced segment. The present research shows that the low vowels resist the trigger to be raised by these voiced consonants preceding them at the word-final position. The low vowel is raised in the case of the first syllable of borrowed words in the language, but retains its [+low] feature in the first syllable of Dravidian words and in the word-final position of native and borrowed words. The theoretical framework of Optimality Theory is employed to understand the constraints working in the language for the phenomenon.
51.	Machine learning-based performance optimization of copper graphene hetero interconnects **S Kushwaha, PR Shamini,** S Roy, D Spina, **R Sharma** - IEEE Transactions on Components, Packaging and Manufacturing Technology, 2026

	Abstract: This work introduces a model-based optimization approach for on-chip copper-graphene interconnects. The aim of this study is to optimize the signal integrity (SI) characteristics of these nano interconnects. Employing existing optimization techniques to improve the SI performance of advanced technology node copper-graphene interconnects remains challenging due to prohibitive computational costs as these interconnects require precise characterization through computationally exhaustive full-wave simulations. Our current work proposes a flexible and efficient modeling and optimization framework that improves SI compared to electromagnetic (EM) simulations using advanced, data-intensive optimization algorithms such as Genetic Algorithm (GA) and Pattern Search. We use the Gamultiobjective and Paretosearch algorithms to demonstrate the capabilities of the proposed framework and verify the accuracy of results in both single- and multiobjective scenarios with the help of two numerical examples.
52.	*N*-annulated [5]helicenes: Syntheses, (anti)aromaticity and properties **HK Saha,** Tarun, **V Kumar,** D Mallick, UK Pandey, **S Das** - Organic Letters, 2026 Abstract: *N*-Annulated [5]helicene (**NH5**) and its dibenzo-extended derivatives are synthesized by cycloisomerization and Scholl-type cyclodehydrogenation methods, respectively. Nitrogen-bridging of *fjord*-carbons 1 and 14 of [5]helicene endows saddle-like **NH5** featuring an antiaromatic azepine core with enhanced orbital overlap between nitrogen and the carbon π-system. *N*-Annulation results in less stabilized HOMO, a smaller HOMO–LUMO energy gap, red-shifted absorption, fluorescence, paratropic ring current over the azepine unit, and tunable aromaticity of the core relative to pristine [5]helicene. The **NH5** derivatives exhibit space-charge-limited current hole mobility on the order of 10^{-3} cm^2 V^{-1} s^{-1}, which is higher than that of *N*-annulated PAH, like *N*-annulated perylene. 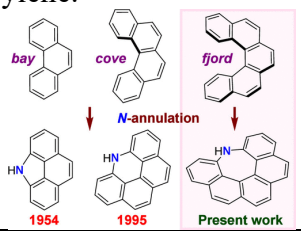
53.	Nonreciprocal magnon splitting and nonlinear spin nernst response driven by magnon-magnon processes S Sharma, M Faizee, **A De Sarkar** - Physical Review B, 2026 **Abstract:** We investigate the influence of magnon-magnon interactions on the nonlinear magnon spin Nernst effect in honeycomb antiferromagnets within the framework of semiclassical Boltzmann transport theory under the relaxation time approximation. To incorporate interaction effects, we examine both three-magnon and four-magnon processes using a combination of perturbative many-body Green's function and mean-field approximations. We compute the interactions-induced modification in the magnon band structure and assess its impact on the nonlinear spin transport. In the case of in-plane Dzyaloshinskii-Moriya interaction, three-magnon scattering processes lead to a nonreciprocal splitting of the magnon spectrum, which remains stable and amplifies the spin Nernst effect in the linear regime. Conversely, four-magnon interactions lead to thermal renormalization of the magnon spectrum, which tends to reduce the nonlinear spin Nernst response. Our findings highlight the crucial role of magnon-magnon scattering in shaping the nonlinear spin response magnetic systems.
54.	Novel copper-thioproline complex as an efficient catalyst for knoevenagel condensation in green solvent: DFT and catalytic activity study SD Khongbantabam…**M Moirangthem,** L Nahakpam, **SK Meena**… - ChemistrySelect, 2026

	Abstract: In this study, we report the synthesis of copper (II) thioproline complex [**Cu(Thp)$_2$**] using optically active ligand L-thioproline in methanolic solvent via conventional reflux method. The complex was characterized by means of elemental analysis, IR, electronic spectra (DRS UV), EPR, magnetic moment measurements, SEM, and PXRD analysis. The structure and geometry optimization of the Cu-thioproline complex [**Cu(Thp)$_2$**] was performed using DFT calculation confirming the formation of distorted square planar geometry. HOMO and LUMO energy gap were also calculated theoretically and found to be 0.21 eV in alpha spin orbitals and 0.11 eV in beta spin orbitals, respectively. The copper (II) thioproline complex [**Cu(Thp)$_2$**] was utilized as a heterogenous catalyst for the Knoevenagel condensation reaction with effective recovery up to fourth catalytic cycle maintaining high activity (above 90% yield) in green solvent ethanol avoiding the use of toxic solvents.
55.	Novel graphical method for uncovering multiple harmonic mitigation solutions at ultra-low switching in multilevel inverters **S Mukherjee, P Kalkal, AVR Teja** - IEEE Transactions on Industrial Electronics, 2026 **Abstract:** This article proposes a novel graphical technique for identifying several sets of switching angle solutions with the same fundamental to mitigate different harmonics in a cascaded H-bridge (CHB) multilevel inverter with ultra-low switching frequency at fixed dc input. This technique is then applied on a three-phase seven-level CHB inverter for mitigating 50 lower-order harmonics with the limitation of three switching angles each quarter cycle. This ensures that the switching frequency is the same as the fundamental frequency. Using this technique, it is demonstrated that in more than 45% region of the available range of modulation indices, with just fundamental switching frequency, a seven-level inverter can mitigate all harmonics from its output line voltage up to the 50th order within the 5% range according to the IEEE 519-2022 standard. Apart from this, more than 20% region also provides a total harmonic distortion below the 8% value. The results obtained from the proposed graphical analysis are verified in simulation using MATLAB/Simulink software as well as hardware using an FPGA-based experimental prototype developed in the laboratory. Typical results are provided with three, four, and five switching angles in seven-level, nine-level, and three-level multilevel inverters respectively to validate the findings.
56.	Numerical investigation of laminar forced convection of shear-thinning fluids through alternating dual orifices **N Dutt, T Mondal, SA Patel** - Journal of Fluid Flow, 2026 **Abstract:** A numerical investigation is conducted to study two-dimensional laminar forced convection of shear-thinning fluids flowing through a pipe equipped with alternating dual orifices under isothermal wall conditions analysed over a wide range of pipe Reynolds number, ($1 \leq Re \leq 100$) for a fixed orifice plate thickness ratio, ($\gamma = 1/16$) and two orifice-to-pipe diameter ratio, ($\beta = 0.2$ and 0.8). The rheological behaviour of the fluid is described using the shear-thinning fluids with the power-law index (n) varying from 0.2 to 1, encompassing strongly shear-thinning to Newtonian fluids. The flow and heat transfer characteristics are analysed in terms of pressure coefficient, streamline patterns, velocity contours, centreline velocity, and local Nusselt number. The results indicate that the formation of vena contracta downstream of the upstream orifice is independent of the presence of the second orifice but is strongly influenced by the orifice diameter ratio. Conversely, the occurrence of vena contracta downstream of the second orifice depends on the diameter ratio. While the downstream flow structure resembles that of a single-orifice configuration, the inter-orifice region exhibits a unique flow pattern characterized by a donut-shaped vortex near the wall and a jet-like core flow. The extent of vortex formation increases with increasing Reynolds number and power-law index for Pr = 0.7, highlighting the combined influence of inertia and shear-thinning behaviour on the thermo-hydrodynamic performance.
57.	Parameter sensitivity and critical transition anticipation in bistable toxin-antitoxin dynamics

	SN Chattopadhyay, IU Irshad, AK Sharma, **AK Gupta** - Computers in Biology and Medicine, 2026 **Abstract:** Toxin–antitoxin systems are central to bacterial persistence, promoting drug tolerance and infection relapse, and therefore demand a clear mechanistic understanding of their regulation. It is thus intriguing to investigate the possible routes to persister cell formation through mathematical modelling and to assess whether their emergence can be anticipated using statistical measures. For this dual purpose, a mathematical model describing the fundamental biochemical interactions among the operon, mRNA, toxin, antitoxin, and two associated protein complexes is considered in this study. The uncertainty in the steady-state behaviour of the deterministic model outcomes is analysed using two complementary forms of global sensitivity analysis. Both these techniques identify six key parameters that substantially influence transcription, translation, and the turnover of antitoxins. Among these, the parameter controlling the quadratic repression of antitoxin through toxin binding has opposite effects on the two species, thereby driving hysteresis between alternate physiological states. Intrinsic noise is introduced into the deterministic model via the chemical master equation. Subsequent Gillespie simulations reveal a critical transition from normal to persister cells, which is then detected using twelve multivariate statistical indicators within moving- and expanding-window frameworks. Sensitivity analyses define hyperparameter ranges that ensure reliable predictions, and robustness tests across repeated simulations show consistent performance for most moving-window indicators, except for some variance–covariance and information-based measures. The expanding-window approach reveals different types of warnings—flickering, sustained, and spurious—quantified by true-positive rates, lead times, and total warning counts. Together, these results demonstrate that multivariate measures can reliably predict critical transitions and provide a solid framework for understanding the loss of resilience in complex biological systems.
58.	Prototypical aggregate network-boosting few-shot learning for medical image classification **RR Chowdhury, U Niyaz, DR Bathula** - Multimedia Tools and Applications, 2026 **Abstract:** Prototypical Networks have proven effective for metric-based few-shot learning, enabling models to generalize from limited labeled examples. However, their application to medical image analysis remains challenging due to the complex, high-variability nature of medical images and the need for robust, domain-specific feature extraction. This work proposes Prototypical Aggregate Network (PANet), an enhanced variant designed specifically for few-shot medical image classification. PANet addresses two key challenges: (a) it incorporates spectral components using Discrete Wavelet Transform (DWT) to explicitly capture texture and frequency information relevant for pathology localization, and (b) it mitigates information loss by aggregating intermediate feature embeddings via depth-wise averaging, allowing downstream layers to benefit from earlier-layer morphological cues. PANet outperforms several state-of-the-art few-shot learning models in low-shot settings, achieving average accuracy gains of 2.8% and 1.55% in 2-way 3-shot and 5-shot classification tasks, respectively, on the BreakHis dataset. Furthermore, it demonstrates statistically significant improvements over comparable architectures and achieves competitive performance against much deeper and more complex models on the PathMNIST and BloodMNIST datasets. Qualitative results using explainability methods further validate PANet's capability to localize and distinguish subtle morphological patterns, enhancing interpretability and supporting its potential for real-world clinical deployment.
59.	Rapid detection of milk adulteration using AI-driven portable colorimetric spectroscopy A Sharma… **R Jana, P Pandey,** R Kumar - Discover Food, 2026 **Abstract:** This study presents a non-destructive, artificial intelligence (AI)-assisted spectro-analytical system for rapid milk adulteration detection using a laboratory-developed portable

	reflectance spectrophotometer operating across 410–940 nm. Six adulterants—urea, formalin, hydrogen peroxide, baking soda, sucrose, and cornstarch—were evaluated individually to establish compositional–spectral relationships within a single-adulterant modelling framework. Physicochemical characterization confirmed adulterant-dependent shifts in solids-not-fat (SNF; 3.29–9.18%), fat (1.5–5.4%), and protein (2.01–3.40%), supporting class-level discrimination. Analysis of variance (ANOVA) revealed active spectral windows at 410–510 nm and 680–940 nm, corresponding to chromophore absorption and near-infrared (NIR) overtone regions. Strong wavelength–property associations were identified, including negative correlations at lower wavelengths ($r = -0.81$ to -0.93) for protein and SNF, and positive correlations at higher wavelengths ($r = 0.74$–0.89) for carbohydrate-based adulterants. Principal component analysis (PCA) explained 91.6% variance, confirming distinct adulterant-specific clustering. ANOVA-based feature selection isolated three discriminatory spectral zones per adulterant. Classification models—Decision Tree, Logistic Regression, support vector machine (SVM), and ensemble methods—achieved ≥ 99% accuracy with inference times below 0.15 ms, with Decision Tree and Logistic Regression offering optimal edge efficiency. The study demonstrates compact, low-cost, AI-enabled multispectral milk monitoring for real-world deployment.
60.	Rapid diagnosis of dengue disease using disposable paper based capacitive sensor G Sarma, **MJ Das**… PP Sahu - Microchemical Journal, 2026 **Abstract:** Rapid and low-cost diagnostic tools are urgently needed for early detection of life-threatening dengue infections, particularly those caused by the prevalent DENV-2 serotype transmitted by *Aedes aegypti*. Although rT-PCR remains the gold standard, its dependence on sophisticated instrumentation and prolonged processing steps limits its applicability in resource-constrained settings. Here, we introduce a new disposable paper-based capacitive biosensor that integrates a novel comb-type interdigitated electrode (IDE) structure with inclined fingers engineered to enhance electric-field overlap, enabling highly sensitive dielectric sensing. The sensor is fabricated on a Whatman paper substrate and employs naringin as a biodegradable molecular recognition layer, selected through molecular docking and experimentally validated via FTIR analysis. Calibration with known serum samples and blind testing of clinical samples yields a sensitivity of 92.3% and specificity of 92.1%. The device requires only 15 µL of sample and delivers the result within 2.5 min representing a substantial improvement over conventional diagnostic assays. Owing to its paper platform and natural citrus fruit extract naringin as a sensing material, the biosensor is fully disposable and environmentally benign. Collectively, these attributes establish this detection platform as a novel, eco-friendly and highly practical point-of-care diagnostic alternative to the existing rapid dengue detection kits. 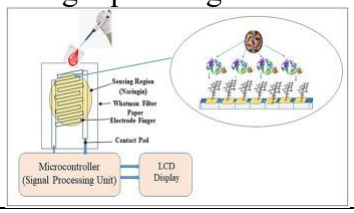
61.	Rate splitting aided multi-user cooperation for next-generation vehicular clusters **S Bhattacharyya, S Darshi,** DT Hoang - IEEE Transactions on Wireless Communications, 2026 **Abstract:** The surge in traffic has amplified the need for greater reliability and higher throughput in vehicle-to-vehicle (V2V) communications. While network-coded cooperation (NCC) offers a promising solution, its reliance on overheard signals and susceptibility to network coding noise raise concerns about the quality-of-service (QoS) being provided. To address this, we propose a rate-splitting aided multi-user cooperation (RSMUC) framework, which employs rate-splitting multiple access (RSMA) as a relaying scheme and enhances the QoS by removing the dependency

	on overheard signals while leveraging the inherent benefits of RSMA. The outage probability analysis of the system is performed, where joint cumulative distribution functions (CDFs) are essential for accurately characterizing the outage performance of both common and private streams. To model the interdependence between these streams, we develop a copula-based framework. The results show close alignment between the simulated results and the derived analytical equations. Comparative evaluations against benchmark schemes, like NCC variants and non-orthogonal multiple access (NOMA) based cooperative systems (NCS), show that RSMUC significantly outperforms existing approaches across various performance metrics like outage probability and throughput. The contribution of RSMA was further verified through comparisons of throughput and packet delivery/drop (%) rates, providing key insights that are crucial in setting vehicular cluster sizes. These findings underscore the potential of RSMUC to enhance reliability and deliver improved QoS in next-generation V2V networks.
62.	SHAPER: SHape-aware parameter-efficient representation learning for medical image segmentation **U Niyaz,** AS Sambyal, **RR Chowdhury, DR Bathula** - Knowledge-Based Systems, 2026 **Abstract:** Medical image segmentation is crucial for healthcare, requiring high accuracy for precise structural delineation. Traditional deep learning methods primarily focus on local features, which can lead to a limited understanding of the global context, and explicitly incorporating it often increases computational costs. To address this challenge, we propose combining the efficiency of Elliptical Fourier Descriptors (EFDs) to represent the global structural characteristics and the Conditional Knowledge Distillation (CKD) framework to selectively transfer relevant information to the low-parameterized student network. We evaluate the effectiveness of our approach and its variants by comparing them with state-of-the-art methods across four benchmark medical imaging datasets. Experimental results demonstrate that our proposed method (V_4) consistently outperforms conventional knowledge distillation approaches. Averaged over the four datasets, it achieves IoU improvements of 1.13%, 2.18%, and 2.15%, and Dice score gains of 0.97%, 1.67%, and 1.44% for the U-NetResNet34, U-NetResNet18, and U-NetMobileNet architectures, respectively. Moreover, the integration of shape prior with knowledge distillation enhances interpretability and provides better uncertainty estimates, further highlighting the robustness and adaptability of our approach. The code is available at https://github.com/UsmaBhat
63.	Strain-modulated tuning of rashba signature and catalytic activity on oxynitride surface: Facet matters **PP Mohanty, R Ahuja,** S Chakraborty - ACS Applied Materials & Interfaces, 2026 **Abstract:** Tantalum-based oxynitride perovskite $SrTaO_2N$ distinguishes itself as a rare semiconducting material, exhibiting remarkable stability in aqueous environments and a narrow band gap, rendering it a highly active catalyst for the hydrogen evolution reaction (HER). In this study, we employ first-principles density functional theory (DFT) calculations to provide mechanistic insights into the electrochemical HER occurring on the low-indexed (001) and (110) surfaces. The computed adsorption free energy of hydrogen adsorption (ΔG_H) for these facets indicates their favorable catalytic activity toward HER. Additionally, a detailed analysis of the system's electronic structure reveals the elemental contribution to both the valence and conduction band edges. The influence of the biaxial strain on enhancing the selectivity of the oxynitride system for hydrogen evolution is also thoroughly examined. Finally, the strain-modulated HER activity is elucidated through changes in the charge profile, providing a deeper understanding of the strain-induced effects on surface charge contribution and catalytic performance.

	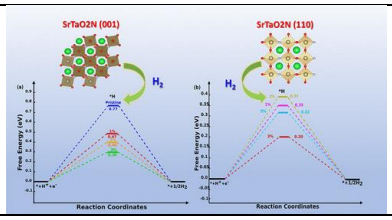
64.	Structure influences case processing: Electrophysiological insights from hindi light verb constructions **AM Mathew,** R Muralikrishnan, M Gulati, **KK Choudhary** - Brain Sciences, 2026 **Abstract:** Background: Case marking serves as a crucial cue in sentence processing, enabling the prediction of upcoming arguments, thematic roles, and event structure. Cross-linguistic studies have revealed language-specific variations in case processing, with differences observed between nominative–accusative and ergative languages, albeit with limited data from the latter. Objective: To this end, we investigated case processing in Hindi compound light verb constructions, leveraging its split-ergative system. Methods: An ERP study was conducted with twenty-four native Hindi speakers, wherein the subject case (ergative or nominative) either matched or mismatched with the aspect marking on the light verb (perfective or imperfective). Results: The results revealed distinct ERP effects depending upon the subject case: a P600 effect for ergative case violations at the imperfective light verb and a biphasic N400-P600 effect for nominative case violations at the perfective light verb. Conclusions: These findings suggest underlying neurophysiological differences in the processing of ergative versus nominative case alignment within light verb structures. Moving forward, a closer examination of structure-specific neurophysiological variation can help bridge the gap between typological distributions and their neural underpinnings.
65.	Synergistic engineering of a cationic polymer–ag catalyst matrix with enhanced electrochemical generation of reactive oxygen species for energy-efficient pathogen inactivation at lab scale and in municipal effluent S Kalra… **N Singh** - ACS ES&T Engineering, 2026 **Abstract:** Commercial wastewater disinfection technologies are inadequate for achieving rapid, durable, and energy-efficient pathogen removal, particularly against high loads of *E. coli* in sewage treatment plant (STP) effluents. In this context, we have developed an engineered material comprising *1-(carboxymethyl)pyridin-1-ium* (IL-5)-functionalized polyethylenimine (PD5) and Ag nanoparticles (PD5-Ag) *via* σ/π–d band interactions. After analyzing its biosafety by cytotoxicity analysis, it was integrated into a chitosan/poly(vinyl alcohol) (CHPV) matrix at varying concentrations. The combined effect of electron modulation of Ag by PD5 *via* σ/π–d band interactions and integration with the CHPV matrix enhances its electrocatalytic activity, rapid reactive oxygen species (ROS) generation, and minimum catalyst loss. The optimized PD5-Ag/CHPV-4 matrix demonstrated high electrochemically active surface area, low Tafel slope, and minimal Ag leaching. Moreover, it achieved complete *E. coli* inactivation within 8 min through a "latch–kill–detach" mechanism and retained 94.7% efficacy after 200 cycles. It effectively disinfected the STP effluent, thereby highlighting its practical applicability as an energy-efficient electro-disinfection platform for safe municipal water reuse. 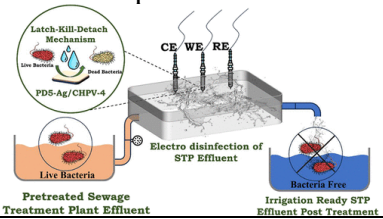

66.	Targeting the Skp1-Skp2 interaction interface with peptide-based inhibitor: Understanding the conformational implications of protein-peptide binding S Tolani, **NM Tripathi**… **A Bandyopadhyay,** A Kumar - Biophysical Journal, 2026 **Abstract:** Peptides have emerged as promising agents to target challenging protein-protein interactions (PPIs). One such difficult interface is the Skp1-Skp2 interaction, which has proven resistant to effective inhibition by small molecules. Here, we rationally designed stapled peptide candidates that effectively disrupt the Skp1-Skp2 interface. Two distinct stapling strategies were employed to enhance peptide stability and potency. The peptides' efficacy was validated using surface plasmon resonance (SPR) and cancer cell line assays, demonstrating their mechanistic impact. To deepen our understanding and identify more potent binders, we examined peptide interactions with Skp1, revealing a stapling-dependent effect on binding affinity. This was further investigated through combined SPR and nuclear magnetic resonance (NMR) spectroscopy analyses. Correlations between NMR relaxation parameters, chemical shift perturbations, and binding affinity allowed us to distinguish enthalpic and entropic contributions influenced by stapling. Leveraging these insights into dynamic changes and their impact on peptide activity, we aim to develop highly effective peptide inhibitors against Skp1-Skp2 and extend this approach to other challenging PPI interfaces.
67.	The cellular harvest: A symbiotic road map for food sovereignty **DA Mosoh,** WA Vendrame - Trends in Biotechnology, 2026 **Abstract:** The 'predatory replacement' model in agriculture is untenable. We propose a symbiotic framework valorizing farmer-supplied agricultural waste side-streams to fuel bioengineered plant callus for decentralized high-value metabolite biosynthesis. Anchored in open-source governance and codesign, this approach shifts from displacement to innovation, reintegrating farmers to enhance sovereignty and resilience.
68.	Tribological behavior of DLC/AlCrN coatings on heat-treated grey cast iron under SAE 10W-30 lubrication G Murari, B Kumar, **SW Khan,** B Nahak, T Pratap - Proceedings of the Institution of Mechanical Engineers, Part J: Journal of Engineering Tribology, 2026 **Abstract:** High contact stress, load, and speed significantly deteriorates the tribological performance of grey cast iron, leads to shorter component life cycle. Heat treatment coupled with coating may significantly enhance component lifespan and tribological performance due to change in substrate physiochemical properties. Thus, this work focused on the influence of heat treatment at 900°C, followed by rapid water quenching, then deposition of DLC and AlCrN coatings. Further, the surface morphology, microstructure, and worn behavior during micro-scratch and tribotest were analyzed. The DLC coating showed highest reduction in friction coefficient (COF) compared to AlCrN due to its high hardness by 36.3, 21.2, and 16.9% under applied load 40N, 80N, and 120N, respectively. A deep abrasion wear was found on the AlCrN coating, whereas a fine wear mark was observed on the DLC coating under all applied load, owing to least COF and chemically inert behavior of DLC. Although AlCrN exhibits relatively higher wear due to surface defects and its brittle nature compared to DLC but its highest hardness helps in reducing COF from untreated substrate highlighting the role of heat treatment in reducing COF. DLC has superior performance compared to AlCrN for volumetric wear, by reducing wear volume loss of about 9.94%, 5.76%, and 5.29% under static loads of 40N and 80N, and progressive loads of 20–120N, respectively whereas material adhesion was more prominent for AlCrN as confirmed from worn surface morphology.
69.	Tuning catalytic activity in nitride perovskite through strain-induced rashba spin splitting manipulation

	P Parimita Mohanty, SH Mir, **R Ahuja,** S Chakraborty - Chemistry of Materials, 2026 Abstract: Rashba spin splitting is an emerging phenomenon originating from the synergistic effect of relativistic spin–orbit coupling (SOC) due to the presence of a heavy constituent element and the noncentrosymmetric crystal structure. We recently observed Rashba spin splitting in the rare nitride perovskite CeNbN3. This work explores how tuning the Rashba spin splitting strength can enhance photocatalytic water splitting and hydrogen evolution reaction (HER) activity. Based on our electronic structure calculations, we have observed the fine-tuning of Rashba spin splitting in CeNbN3 under the influence of compressive strain and the corresponding impact on HER activity. The evolution of electronic band structure, Rashba spin splitting strength, and spin texture under compressive strain corresponds well with the hydrogen adsorption free energy determined from the constructed reaction coordinate mapping of the HER mechanism. The strength of spin splitting shows a correlation with improved HER activity, which is in line with the influence of the Rashba effect. 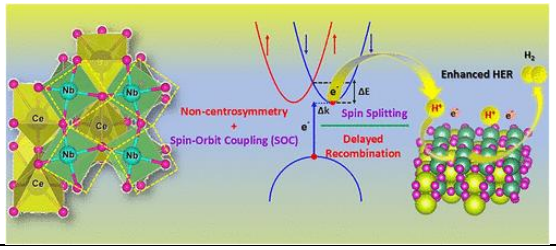
70.	Utilization of bulk nanobubbles to influence combustion characteristics of liquid fuels **V Kurumanghat, A Sharma, N Nirmalkar,** A Saurabh, **L Kabiraj** - Applications in Energy and Combustion Science, 2026 **Abstract:** Several reports have recently established the possibility of stable suspensions of bulk nanobubbles in liquids, thus opening new directions in a broad range of applications including power and propulsion applications that depend on liquid fuels. In this article, we report our investigation on bulk nanobubble suspensions of oxygen and nitrogen/air nanobubbles in isopropyl alcohol (IPA), ethanol, Jet A-1, and petrol. Bulk nanobubbles were generated by hot and cold solvent mixing method. Physical properties of the suspensions thus obtained were characterized in terms of the surface tension, zeta potential, bubble size distribution, and the mean bubble size. The stability of the suspension was tracked over a duration of three days. Finally, the combustion performance of the various fuel suspensions was investigated through single droplet combustion experiments. Results show successful generation of nanobubbles in all four fuels. IPA showed the highest bubble concentration. Bubble concentration decreased over time for all fuels. Droplet combustion studies revealed that the presence of nanobubbles led to a reduction in the burning rate constants for IPA, ethanol, and petrol, and an increase in burning rate constant for Jet A-1. Nanobubble suspensions are found to exhibit an increased frequency and intensity of bubble growth and bursting events, which in turn induced larger disturbances on the droplet interface in comparison to the pure fuels.
71.	Yttrium-modified polymer-derived SiOC ceramics with enhanced high-temperature thermal stability **SR Kumar, RM Prasad** - Ceramics International, 2025 **Abstract:** In this work, polymer-derived silicon oxycarbide (SiOC) ceramics and yttrium-modified silicon oxycarbide (SiOC/Y) ceramic composites were synthesized via pyrolysis of as-received polymethylsilsesquioxane (PMS) and PMS-modified with yttrium acetate, respectively, in the temperature range of 1000–1600 °C. The obtained ceramics were subjected to microstructural analysis using FTIR spectroscopy, XPS, Raman spectroscopy, XRD, and FESEM.

	At high temperatures (>1100 °C), yttrium oxide formed from the decomposition of yttrium acetate reacted with amorphous silica present in the SiOC matrix and forming yttrium silicates in the composites. Synthesized SiOC and SiOC/Y ceramic particles were found to be spherical in shape; in SiOC/Y, yttrium silicate precipitated on the SiOC particles. The obtained SiOC/Y composites displayed high thermal stability compared to SiOC ceramics at 1600 °C by impeding carbothermal reduction.
72.	Zeros of harmonic polynomials **K Jaglan, A Sairam Kaliraj** - Bulletin of the Malaysian Mathematical Sciences Society, 2026 **Abstract:** In their groundbreaking work, Khavinson and Świątek proved Wilmshurst's conjecture, establishing a sharp upper bound on the number of zeros of harmonic polynomials of the form $h(z)-\bar{z}$, where h(z) is an analytic polynomial of degree greater than one. Recently, Dorff et al. determined the number of zeros, while Liu et al. identified the compact region containing all zeros of harmonic trinomials. In this article, our research takes a leap further in identifying the precise compact region encompassing all zeros of general harmonic polynomials. Moreover, we utilize the harmonic analog of the argument principle to explore the distribution of zeros of these polynomials, offering insightful examples for clarification.

Disclaimer: This publication digest may not contain all the papers published. Library has compiled the publication data as per the alerts received from Scopus and Google Scholar for the affiliation "Indian Institute of Technology Ropar" for the month of February, 2026. The author(s) are requested to share their missing paper(s) details if any, for the inclusion in the next publication digest.